IEEE Access
Multidisciplinary | Rapid Review | Open Access Journal

Received June 10, 2020, accepted June 30, 2020, date of publication July 3, 2020, date of current version July 16, 2020.

Digital Object Identifier 10.1109/ACCESS.2020.3006865

Design and Optimize of a Novel Segmented Soft Pneumatic Actuator

FEI YANG[1], QI RUAN[1], YIMING MAN[2], ZHIJIE XIE[1], HONGHAO YUE[1], BING LI[3], (Senior Member, IEEE), AND RONGQIANG LIU[1], (Member, IEEE)

[1]School of Mechatronics Engineering, Harbin Institute of Technology, Harbin 150080, China
[2]China Academy of Launch Vehicle Technology Research and Development Center, Beijing 100076, China
[3]School of Mechanical Engineering and Automation, Harbin Institute of Technology (Shenzhen), Shenzhen 518055, China

Corresponding author: Zhijie Xie (xiezhijie@hit.edu.cn)

This work was supported in part by the National Science Foundation for Young Scientists of China under Grant 51705098, and in part by the Joint Funds of the National Natural Science Foundation of China under Grant U1613201.

ABSTRACT This article proposes a novel soft pneumatic actuator inspired by the segmented structure of earthworms. The actuator adopts a new structure of free bottom to eliminate the constraint of the bottom and enlarge the bending capacity of the actuator. Through simulation, it is found that the new actuator improves the bending angle by 20% and output force by 40% compared with traditional actuator. Moreover, key parameters of the actuator are analyzed to acquire their effect on bending angle and bending linearity. A guideline for the design and optimization of the actuator is proposed. To validate the simulation results, we build up a test platform to test bending angle and output force of the actuators, the results shows that errors between the simulation and the test remained in the limit of about 10%. Finally, a three-jaw soft gripper is fabricated and its grasping strategy is studied. The quantitative analysis shows its excellent adaptability and load capacity.

INDEX TERMS Soft actuator, parameter optimization, soft gripper, grasping strategy.

I. INTRODUCTION

Flexibility of animal organs such as the elephant trunks and earthworms inspires the development of soft robot. With high flexibility, safe interaction and passive compliance, soft robots are promising in applications such as healthcare industry, picking system of logistics and capturing mechanism. Based on the drive mode, soft robots can be categorized into various types including rope driven soft robot [1], pneumatic driven soft robot [2]–[4], shape memory alloy driven soft robot [5], [6], shape memory polymer driven soft robot [7], [8] and chemical energy driven soft robot [9], [10]. Compared with other types, pneumatic driven soft robots have several advantages including simpler structure, lower cost, faster reaction speed, larger deflection, larger output force. Besides, it is eco-friendly, making it more suitable for modern industry [11]–[14].

The structural design, parameter optimization, modelling method and fabrication method of the pneumatic actuator have been wildly studied [15]. For instance, pneumatic artificial muscle (PAM) is one typical soft pneumatic actuator [16]. It is mainly composed of a continuous rubber tube with a number of fiber ropes enwounding its surface. Fiber ropes can limit the expansion of the rubber tube while enable it to contract, elongate or twist. To further simplify the complicated fiber ropes, the structure of soft pneumatic actuators was proposed [17]. This soft pneumatic actuator is also mainly composed of a continuous rubber tube while it has a strain limiting layer attached to the bottom of tube. This strain limiting layer is mainly made of paper or plastic which can bend yet cannot elongate. When pressurized, the actuator can bend toward one side. These continuous soft actuators have symmetric structures that limit their bendability, and brings other drawbacks such as large energy consumption, low energy output density and slow reaction speed. To resolve these issues, the segmented soft actuator (SSA) was proposed [18]. SSA has good environment adaptability and large capture space, and has been successfully applied in engineering. A number of segmented soft robots have been developed such as starfish shaped soft robots that can be applied in capturing fragile or light objects [19], soft pneumatic rehabilitation gloves composed of 5 actuators [20], soft grippers that can be used for adaptive grasping [21]–[24]. Previous studies of SSA shows its great potential in future industrial application since it exhibites fast reaction speed, large bending angle and grasping adaptability. However, studies on output force

The associate editor coordinating the review of this manuscript and approving it for publication was Wai Keung Fung.

and stiffness assurance of the SSA are insufficient [25]–[27], these limits its industrial application. Therefore, this paper proposes a new structure of the SSA aiming at improving the bending angle and the output force, and finally promotes the application of the actuators.

The traditional SSAs are mostly bottom constrained actuators (CBA). Structure analysis reveals that the constrained bottom significantly impacts the performance of the actuator. We proposes the free bottom actuator (FBA) to overcome this problem. Through finite-element simulation, it is found that the FBA can significantly improve bending ability and output force compared with the CBA under the same pressure. To gain insight of the response of the critical parameter and to efficiently optimize the parameter of the actuator, a finite-element method (FEM) model was established. In addition, several actuator samples were developed and a test platform was established for experiments, and then the simulation results were verified. Finally, a soft pneumatic gripper composed of three actuators was developed, which is capable of capturing several irregular objects with different capturing strategies. Its capturing ability was also tested.

II. DESIGN AND FABRICATION

A. ACTUATOR DESIGN

An SSA is commonly composed of chamber, plate 1, strain limiting layer and plate 2, as shown in Fig.1 (a). The strain limiting layer is made of paper, and all the other components are made of rubber. As the strain limiting layer can only be bent but not be stretched, the actuator bends toward one side when the chamber is expanded with pressure. When reading the bending angle of the actuator, it is assumed that bending of the actuators is equal curvature bending. For soft capturing mechanism composed of multiple soft pneumatic actuators, it forms an enclosure space and applies the force to the surface of the grasped object under the actuation of pressure.

As shown in Fig.1 (b), intervals between each units of CBA are totally fastened to plate 1, with narrow networks at the bottom of the chamber for connection. Analysis reveals that the bonded intervals have large influence on the bending of the actuator as the whole plate is divided into several independent units which strengthens the stiffness. This constraint limits the bending angle of the actuator. This paper proposes a novel FBA to solve this problem. As shown in Fig.1 (c), the FBA has pneumatic networks going through the bottom of the chamber. When fastened to plate 1, only the outer bottom is bonded, leaving the intervals free. Fewer constraints between the intervals and plate 1 allow the actuator to have larger bending angle.

According to previous studies [17], [26], size of the actuator is set as 139mm×24mm×29mm. Each actuator module is composed of several independent chamber units. Key parameters of the actuator is shown in Fig.1 (d), including the number of chamber unit n, interval between chamber unit d, height of chamber section h, width of chamber section b, thickness of chamber t_1, and thickness of plate t_2.

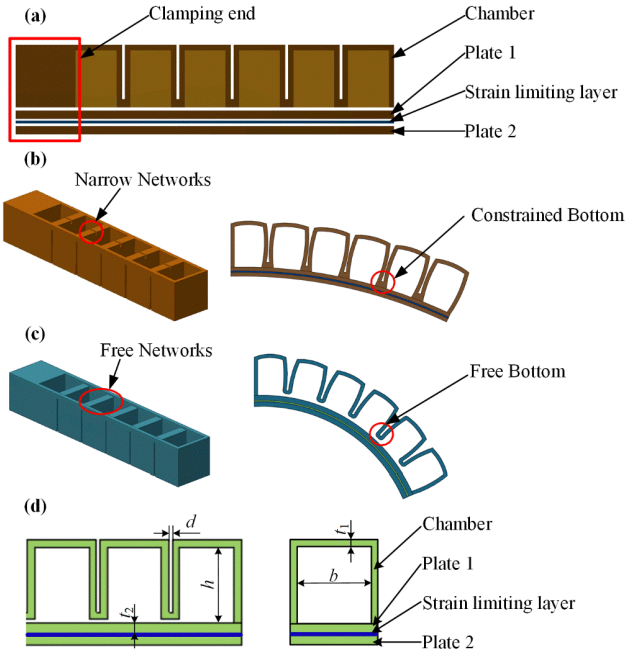

FIGURE 1. (a) Common components of the SSA. (b) CBA with narrow networks and its constrained bending. (c) FBA with free networks and its free bending. (d) Key parameters of the soft actuator.

B. FABRICATION METHODS

The strain limiting layer is made of paper, other components are made of the same type of rubber (Dragon Skin 30, Smooth-on Inc., PA, USA). In order to simplify the fabrication, the rubber component is divided into 3 parts: the chamber, plate 1 and plate 2. All these parts are manufactured with multistep molding process. Molds of the components are all 3D printed by an Allcct 300 printer (Wuhan Allcct Inc., China). After each component is fabricated, the chamber, plate 1, strain limiting layer and plate 2 is adhered successively with Sil-Poxy(Smooth-on Inc., PA, USA), a tube is adhered to the clamping end as the entrance of airflow. Manufacturing process of the actuator is shown in Fig.2.

Dragon Skin 30 is mixed with equal quantity of constituent A/B. During the mixing process, plenty of air may get in since the rubber has high viscosity. In order to improve the performance of the rubber, the rubber should be degrassed twice. The first treatment is pretreatment, occurring just after the mixing of constituent A/B; the second treatment aims at improving the performance of the rubber, which occurs after pouring the mixed rubber into molds. The rubber should be placed under vacuum at 10kPa for 2∼3 minutes during each treatment. It should be noticed that the first treatment can produce plenty of bubbles, so the treatment should be done in a large container in case of the outflow of the rubber.

C. MATERIAL CHARACTERIZATION

Previous studies show that the Young's modulus of Dragon Skin 30 is $E = 1$MPa [1]. However, Young's modulus alone cannot refer to the performance of rubber accurately. Usually, property of rubber was expressed with multiple parameters

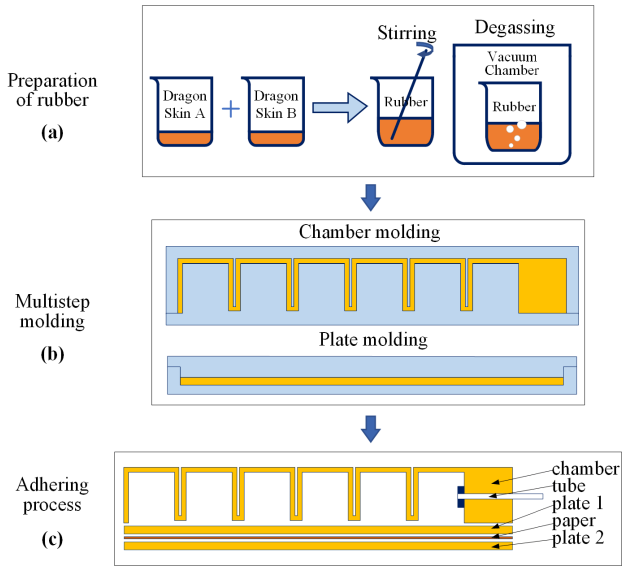

FIGURE 2. (a) Mixing and degassing process of rubber. (b) Multistep molding process of the components. (c) Adhering process of the components.

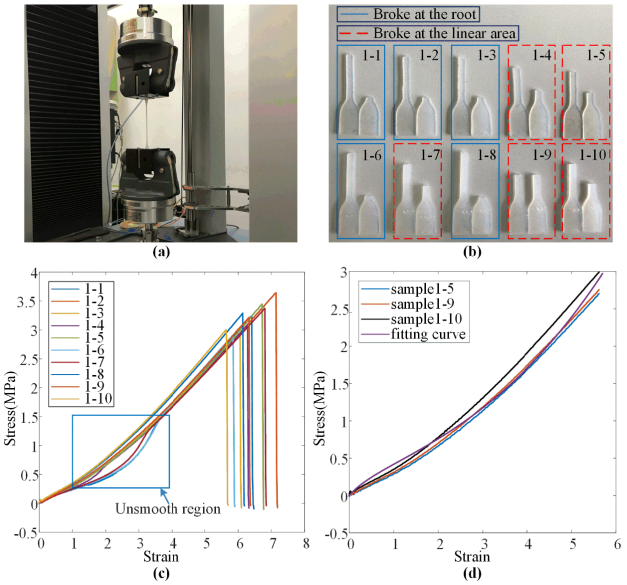

FIGURE 3. (a) Tensile test of rubber. (b) Broken samples after tensile test. (c) Testing curves of rubber samples. (d) Fitting curve compared with testing curves of effective samples.

according to different constitutive models [21], [28]. Therefore, the property of Dragon Skin 30 should be calibrated. Samples were fabricated and tested according to ISO37-2005. Besides, in order to reduce manufacturing error of the samples and ensure the correctness of testing, 10 samples were fabricated and used for tensile test. Process of the tensile test and broken samples are shown in Fig.3 (a) and Fig.3 (b). It can be seen that the root and the linear area of the samples may be broken. Samples broken at the linear area was chosen for analysis (1-4/ 1-5/ 1-7/ 1-9/ 1-10).

Rubber can be seen as an incompressible material approximately. A second order hyperelastic incompressible Yeoh material model is used to analyze bending of the actuator as (1).

$$U = \sum_{i=1}^{2} C_i \left(I_1 - 3\right)^i \tag{1}$$

I_1 is the first deviatoric strain invariant, and C_1, C_2 are the material-specific coefficients [15]. The relationship between stress and strain is shown as (2), where σ and λ are the engineering stress (MPa) and stretch ratio respectively.

$$\sigma = 2 \times \left(\lambda - \frac{1}{\lambda^2}\right) \times \left[C_1 + 2C_2 \left(\lambda^2 + \frac{2}{\lambda} - 3\right)\right] \tag{2}$$

Fig.3 (c) shows the stretch curves of the samples. It can be inferred that several curves with obvious unsmooth region may have larger error in parameter fitting. Therefore, tensile samples with smooth curves were chosen to analyze (1-2/ 1-3/ 1-5/ 1-8/ 1-9/ 1-10). Comprehensively considering the broken region of the samples, tensile data of these samples (1-5/ 1-9/ 1-10) were analyzed and fitted. The experiment data with an elongation of 0∼570% was imported to Matlab and plotted their curves. Using (2) to fit the curves, an average result was obtained with $C_1 = 0.11488$Pa, $C_2 = 0.001262$MPa. The fitting curve compared with the testing curves of effective samples is shown in Fig.3 (d).

III. FEM SIMULATION

A. FEM MODELLING

With high material nonlinearity and deformation nonlinearity, it is difficult for pneumatic actuator to achieve accurate analytical solution. FEM is a common analysis method with high accuracy for soft robot [18], [28]. Through FEM simulation, input and output characterization of the CBAs and the FBAs can be acquired, which can be used for structure improvement and parameter optimization.

FEM models of the CBAs and the FBAs were developed using ANSYS. Since the clamping end has no contribution to the bending of the actuator, it was simplified in the simulation model to improve the compute efficiency. As described earlier, components such as the chamber, plate 1, plate 2 are made of Dragon Skin 30. They were modelled with solid tetrahedral quadratic elements SOLID 184. The strain limiting layer is made of paper and modelled with shell elements SHELL181. Paper has a linear elastic characterization with Young's modulus of $E = 1.2$GPa, a Poisson's rate of $\mu = 0.2$, and thickness of $\delta = 0.09$mm. All these components are adhered in sequence and the constraints between each component can be seen as bonded. Elements of the contacted surfaces share the same nodes with each other. Additionally, adjacent surfaces of each chamber unit would interact under a certain pressure. Hence, frictional constraints should be applied to the adjacent surfaces. Considering the bearing capacity and simulation convergence, pressure loads ranging from 0kPa-25kPa with an interval of 5kPa were applied to the actuators. Bending angle and output force of the actuator were simulated.

B. SIMULATION RESULTS

Bending simulation results of the CBAs and FBAs are shown in Fig.4 (a)- Fig.4 (c). Several researchers test coordinate

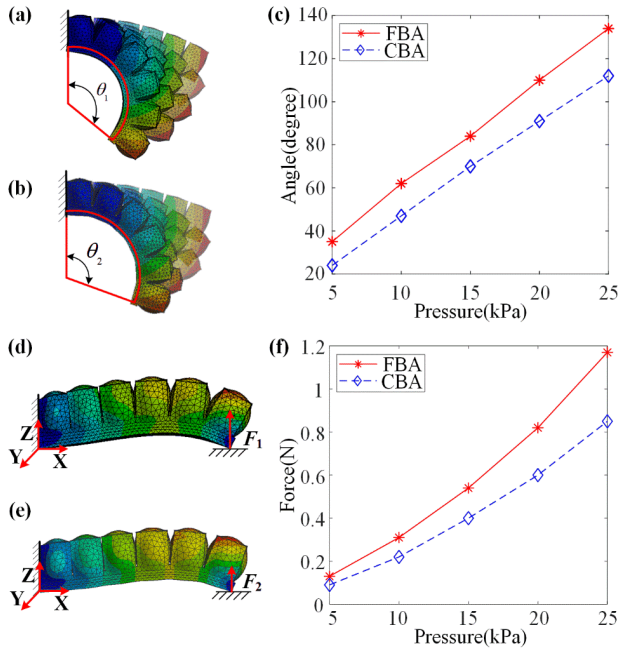

FIGURE 4. (a) Bending simulation results of FBA. (b) Bending simulation results of CBA. (c) Contrast of bending ability for different actuator. (d) Output force simulation results of FBA. (e) Output force simulation results of CBA. (f) Contrast of output forces for different actuators.

values of the distal end to calculate the bending angle of the actuators because the length of the strain limiting layer remains constant. However, this method is based on the hypothesis that center of the circle is on the surface of the constrained surface. Through simulations and experiments it is found that the center would offset from the constrained surface because of the hyperelastic of the rubber chamber. It makes it unsuitable to calculate the bending angle. In this paper, a new method is used to acquire bending angle of the actuators. Bending results were imported into CAD; an arc was plotted to fit bending of the strain limiting layer, and the angle of the arc θ was read as bending angle of the actuator.

It is implied in Fig.4 (a)- Fig.4 (b) that an arc fits well with the bending of the strain limiting layer, proving the hypothesis of equal curvature bending. Bending of the whole actuator is driven by the expansion of each chamber unit. Except for the constrained unit, all the other units have the same deformation. Expansion of all the adjacent surfaces of each unit determines the bending of the whole actuator, so the influence of other surfaces can be ignored.

Comparing Fig.4 (a) with Fig.4 (b), it is obvious that bending angle of the FBA has been significantly improved compared with that of the CBA, demonstrating the advantage of the FBA in bending angle. It can be concluded from fig.4 (c) that bending angle of both the two actuators has a linear increase with pressure, while their ratios remain constant. Under the pressure of 25kPa, bending angle of the FBA reaches 134° while the CBA reaches 112°. Bending angle of the FBA increases by about 20% in average from that of the CBA.

In output force simulation of the actuators, total reaction force of nodes on the bottom edge of the free end was read as output force of the actuator. Output force simulation results of the CBAs and FBAs are shown in Fig.4 (d)- Fig.4 (f). From Fig.4 (d)- Fig.4 (e), it can be seen that both actuators have a similar bending tendency: plate of the actuators bends under the constraints and pressure; chamber units expand while the unit on the far right side has the largest expansion because of the least constraints. From the right side to the left side, expansion of the chamber units decreases in sequence and the unit on the far left side severely extrudes. When comparing Fig.4 (d) with Fig.4 (e), it can be concluded that the FBA generates larger expansion than the CBA under the same pressure, which enables FBA to have a larger output force. As shown in Fig.4 (f), output force of both actuators also has a nearly linear increase with pressure. The increasing tendency of output force almost remain the same as bending angle of the actuators. Under the pressure of 25kPa, output force of the FBA reaches 1.17N while the CBA reaches 0.85N. Output force of the FBA increases by about 40% in average from that of the CBA.

Through FEM analysis, it is obvious that the FBA has better performances in bending ability and output force than that of the CBA. This makes it more suitable for modern industrial application. On the basis of this FBA, soft pneumatic mechanism with higher performance can be developed.

C. PARAMETERS OPTIMIZATION

To further improve the performance of the soft pneumatic actuator and deepen the understanding of its characterization, key parameters of the FBA are analyzed and optimized. As the actuator is modularly designed, it can be multi-module assembled into a capturing mechanism. Hence, the length is not the key parameter and it is kept constant at $L = 139$mm. Optimized key parameters are diplayed in Fig.1 (d), including the width of section b, thickness of chamber t_1, thickness of plate t_2, number of chamber unit n, interval between chamber units d and height of section h. Specific variable selections are listed as follows.

1) Width of section b: 20mm, 25mm, 30mm;
2) Thickness of chamber t_1: 2mm, 3mm, 4mm;
3) Thickness of plate t_2: 2mm/3mm/4mm;
4) Number of chamber unit n: 5, 6, 7;
5) Interval between chamber units d: 1mm, 2mm,3mm;
6) Height of section h: 16mm, 21mm, 26mm.

Through simulation, according to effect on bending of the actuator, mainly include bending angle of the actuator and linear relationship between deformation and pressure,, the structure parameters can be divided into primary influence parameters (b, t_1, t_2) and secondary influence parameters (n, d, h). The simulation results are as follows.

1) PRIMARY INFLUENCE PARAMETERS

a: WIDTH OF SECTION b

Fig.5 (a) shows the influence of section width b to the bending of the whole actuator. As shown in Fig.5 (a), for $b = 20$mm,

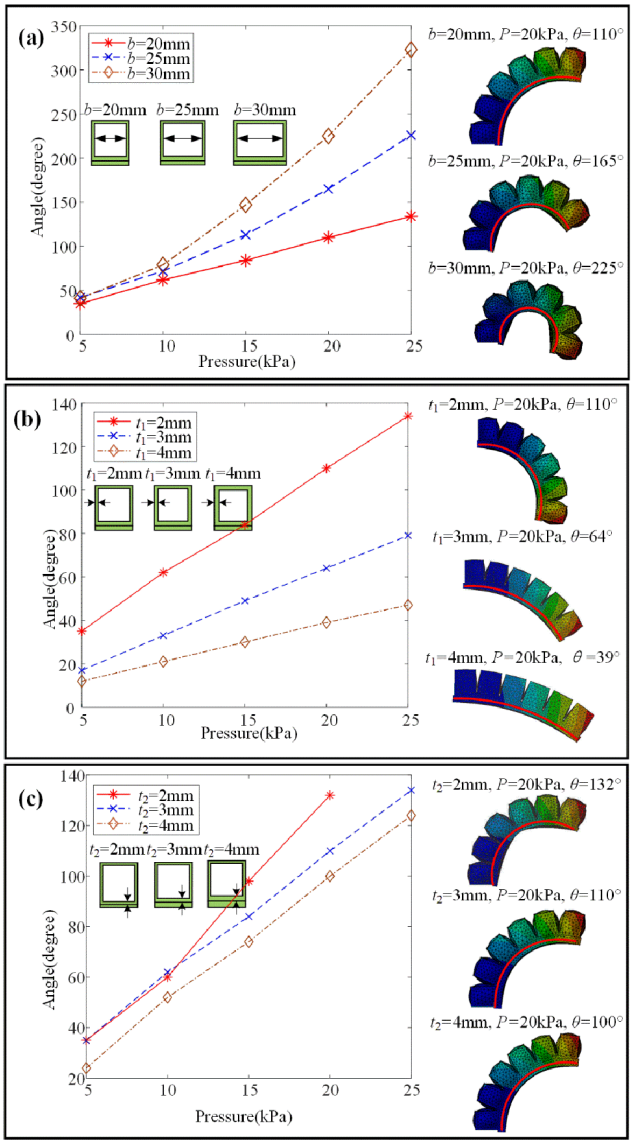

FIGURE 5. FEM simulation results of primary influence parameters. (a) Specific value of 20mm, 25mm, 30mm for width of section *b*. (b) Specific value of 2mm, 3mm, 4mm for thickness of chamber t_1. (c) Specific value of 2mm, 3mm, 4mm for thickness of plate t_2.

bending of the actuator has always a nearly linear relationship with pressure, while for $b = 25$mm and $b = 30$mm are not so. Once the pressure exceeds a critical value, bending angle of the actuator dramatically increases with the growth of section width.

The reason for this phenomenon is mainly because the increase of section width leads to the decrease of length-width ratio and makes the plate more prone to plane deformation. Once the pressure exceeded a critical value, the plate incurs plane deformation accompanied with bending deformation, and curvature of the actuator is no longer an approximate equal ratio. Although growth of section width could enlarge bending angle of the actuator, the possibility of buckling of the plate also increases, and bending angle of the actuator no longer has an approximate linear relationship with pressure, which makes the accurate control difficult. To handle this issue, the section width should be as wide as possible, meanwhile it should assure that under a limitation of pressure, bending angle of the actuator has a linear relationship with pressure. Finally, section width was set to be $b = 20$mm.

b: THICKNESS OF CHAMBER t_1

Fig.5 (b) indicates the influence of the chamber thickness on the bending angle of the actuator. As shown in Fig.5 (b), bending angle of the actuator shows a linear relationship with pressure for different chamber thickness. Bending angle of the actuator is inversely proportional to chamber thickness. Higher thickness leads to better deformation resistance and larger pressure carrying capacity. However, the actuator is less flexible and the bending angle decreases. When the stiffness and pressure bearing capacity of the actuator are maintained, the section thickness should be as small as possible to reduce weight and improve bending ability. As shown in Fig.5 (b), section thickness is set as $t_1 = 2$mm.

c: THICKNESS OF PLATE t_2

Fig.5 (c) shows the influence of the plate thickness on bending angle of the actuator. It indicates that when $t_2 = 2$mm, minor plate thickness leads to insufficient bottom stiffness, and the actuator no longer shows a pure bending deformation because of the plane deformation of the plate. Moreover, while the pressure exceeds 20kPa, the simulation result does not converge. While for $t_2 = 3$mm and $t_2 = 4$mm, bending angle of the actuators has a linear relationship with pressure, and with the increase of plate thickness, bending angle of the actuator drops. In order to keep a linear relationship between bending angle with pressure and to ensure the softness of the actuator, thickness of the plate is set as $t_2 = 3$mm.

2) SECONDARY INFLUENCE PARAMETERS

a: NUMBER OF CHAMBER UNIT n

As shown in Fig.6 (a), with the increase of the number of chamber units, bending angle has a slight increase, since bending of the whole actuator is driven by the deflection of each unit, when the length of actuator remains constant, the equal bending length remains unchanged. Meanwhile, the increase of chamber units results in bigger intervals between each unit which leads to the reduction of the stiffness, and finally the bending angle has a slight growth. Excessive chamber units may increase the failure rate of the manufacture of the actuator. Considering the flexibility and manufacturability, the number of chamber units is set as $n = 6$.

b: INTERVAL BETWEEN CHAMBER UNITS d

As shown in Fig.6 (b), the change of intervals between each chamber units slightly influence the bending angle of the actuator. When intervals increases, although the equal bending length decreases, the stiffness between each connection

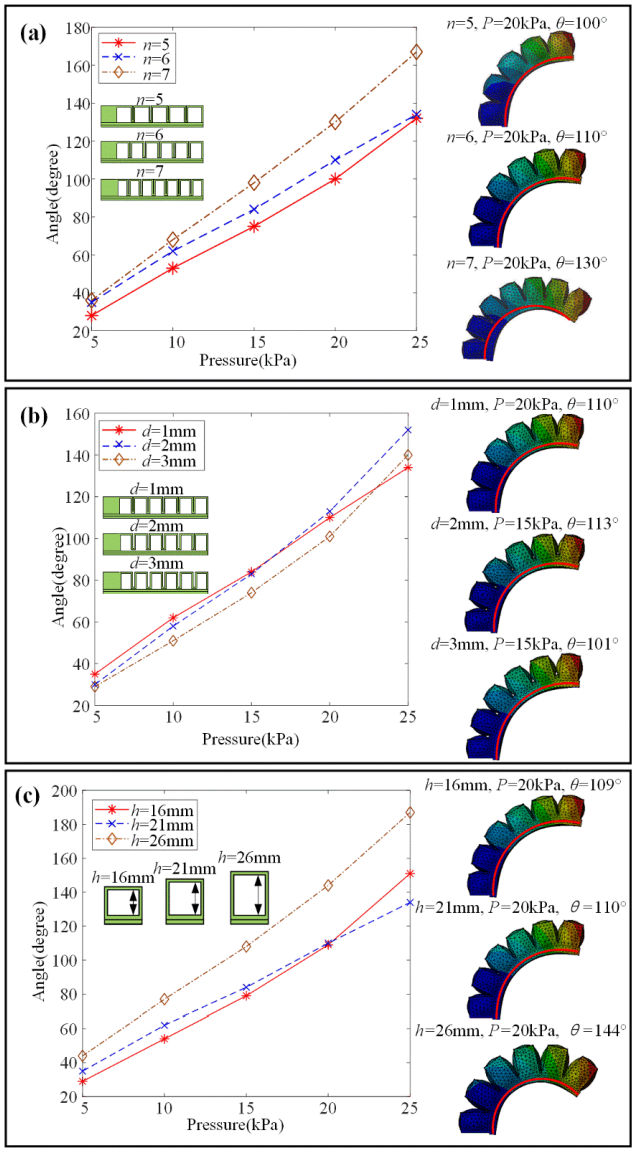

FIGURE 6. FEM simulation results of secondary influence parameters. (a) Specific value of 5, 6, 7 for number of the chamber *n*. (b) Specific value of 1mm, 2mm, 3mm for interval between chambers *d*. (c) Specific value of 16mm, 21mm, 26mm for height of section *h*.

of the units and the interaction between each adjacent face also decline, leading to a nearly constant bending angle of the actuator. Intervals between chamber units is set as $d = 1$mm, considering the stiffness of the actuator.

c: HEIGHT OF SECTION h

As shown in Fig.6 (c), bending angle of the actuator increases along with the increase of the section height. The increase of section height enlarges the total load on the sections and raises the driving moment. Resistance moment of the lateral surface also increases. These two moments offset with each other, so the influence of section height becomes minor. Considering the manufacturability and bending ability of the actuator, height of section is set as $h = 21$mm.

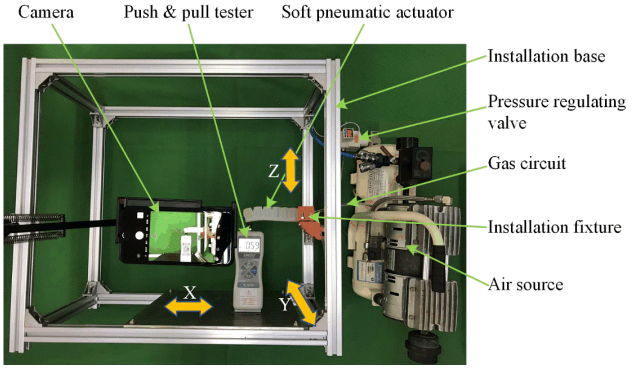

FIGURE 7. Components of the test platform, overhead view.

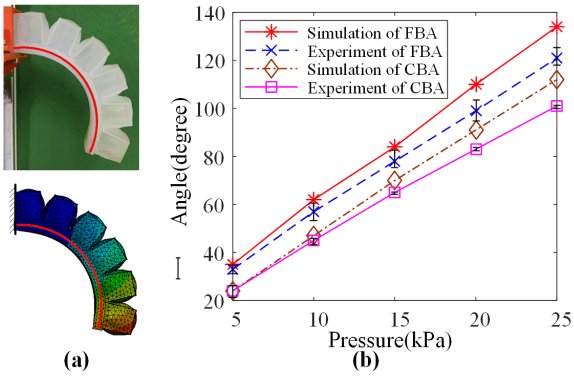

FIGURE 8. (a) Bending results of both test and simulation of a FBA in 25kPa. (b) Test and simulation results comparison of bending angle in the range of 0kPa-25kPa.

IV. CHARACTERIZATION TEST

A. TEST PLATFORM

A test platform was set up to verify the simulation results. The segmented structure leads to low stiffness in the curved plane of the actuator. Therefore, the actuator was horizontally installed with its bending plane parallel to the horizontal plane to reduce the impact of gravity. The platform is mainly composed of the soft pneumatic actuator, a installation base, a installation fixture, a air source, a gas circuit, a manual pressure regulating valve, a camera, and a push & pull tester, as shown in Fig.7. The installation base is the foundation of installation, which can be adjusted according to different requirements. The air conditioning system consists of the air source, gas circuit and the manual pressure regulating valve, enabling the air pressure inside the actuator continuously manual adjustable. There is a display screen on the pressure regulating valve to ensure pressure control of the actuator. The camera records the deformed state of the actuator, and these data are imported into CAD. When taking photos, the camera should be perpendicular to the bending plane of the actuator. The push & pull tester is used to test the output force of the actuator.

To reduce the impact of machining errors and test errors, three FBAs and CBAs were fabricated according to parameters referred above. Pressure loads ranged from 0kPa-25kPa

with an interval of 5kPa were tested respectively, each point triple. Finally, average values were compared with the simulation results to verify the correctness.

When the tests were completed, a soft pneumatic mechanism assembled with these 3 actuators was developed, and its grasping characterization was quantitatively analyzed.

B. BENDING CHARACTERIZATION TEST

The clamping end of the actuator was fixed with installation fixture and the other end was free when testing the bending ability. Bending status were recorded after the actuators were pressurized and maintained stable. According to the method mentioned above, bending pictures were imported to CAD, and an arc was plotted to fit the bending of the strain limiting layer, and the bending angle was read.

Fig.8 (a) illustrates the comparison of the test and simulation results of a FBA under the pressure of 25kPa. The test and simulation results are almost the same. Arcs fit well with the bending of the strain limiting layers, which further proves the hypothesis of equal ratio of curvature. The bending of the actuator is composed of that of all the chamber units. The bending of each unit is the same with simulation. Gravity can cause deformation in the vertical direction, but its effect on the horizontal direction can be ignored.

Fig.8 (b) shows that the simulation results of both the CBAs and FBAs fit well with the test results. However, errors between the test results and the simulation results still exist and both of the simulation results are slightly larger than that of the test results. The errors remain in the limit of about 10%. This is mainly due to the manufacture error of the actuator and the test error. The fitting curve can also leads to further error. Though the arc can fit well with the strain limiting layer, but it is still an approximation method, this leads to error of the results.

C. FORCE CHARACTERIZATION TEST

The clamping end of the actuator was fixed with installation fixture and the other end was supported by the push & pull tester when testing the force characterization. Before the test, the installation position of the tester was adjusted to made the free end just contacted with it. With the support of the fixture and tester, an output force can be read, and this force was the output force of the actuator.

Fig.9 (a) shows the results of bending and output forces under the pressure of 25kPa. The actuators have similar test and simulation results under the same pressure. The plates are deflected under constraints, inflation of the chamber units decreases from right to left as the constraints increases.

As shown in Fig.9 (b), simulation results and test results of the FBAs and CBAs fit well in output forces of the free end. The errors between the simulation results and test results remain within 10%. There exist two major causes to the error. Firstly, structure parameters such as thickness of the chamber have manufacture errors, while these parameters have standard value within simulation. Secondly, support of the free end is approximately treated, which may has slight distinction with test.

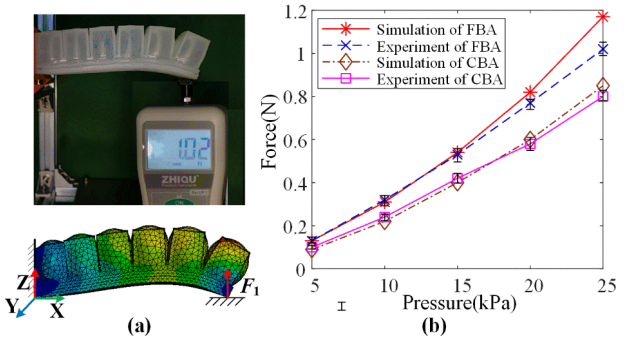

FIGURE 9. (a) Output forces and deformation of both experiment and simulation of the actuators in 25kPa. (b) Test and simulation results comparison of output forces in the range of 0kPa-25kPa.

TABLE 1. Comparison of capacity of the actuators.

	Maximum working pressure(kPa)	Bending angle (degree)	Output force (N)	material
This work	40	202.3	2.12	DS 30
Mosadegh *et al.* [18]	72	360	1.4	Elastosil M4601
Polygerinos *et al.* [20]	50	320	1.21	Elastosil M4601
Park *et al.* [30]	80	200	2.56	DS 30+ ABS P430
Polygerinos *et al.* [17]	230	320	8.3	Elastosil M4601+ fiber

Above all, simulation results of the FBAs and CBAs fit well with their test results, this means FEM could be an effective method in structure design and parameter optimization.

D. COMPARISON OF THE SOFT ACTUATORS

Table 1 shows a comparison of the maximum working pressure, bending angle and output force of our new segmented actuator with other soft pneumatic actuators.

In table I, capacity of the traditional segmented actuators [18], [20], the hybrid structured actuator [29] and the fiber reinforced soft actuator is compared with our new segmented actuator. These five actuators have similar structure parameters and material parameters. As it is shown, the maximum working pressure of the new actuator is 40kPa, the bending angle reaches 202.3 degree and the largest output force is 2.12N. Compares with the traditional segmented actuators, its maximum working pressure and bending angle are inadequate, but its largest output force has a significant improvement. The main reason for the inadequate of the maximum working pressure is mainly because of the defect of the adhesive joint, this can be optimized in future works. While compares with the hybrid structured actuator, the new actuator can achieve a similar bending angle and output force with half pressure. Moreover, hybrid structured actuator is a mixture of soft materials and rigid structure, it has a more complex structure and manufacturing process. The fiber reinforced soft actuator shows a much higher output force than that of

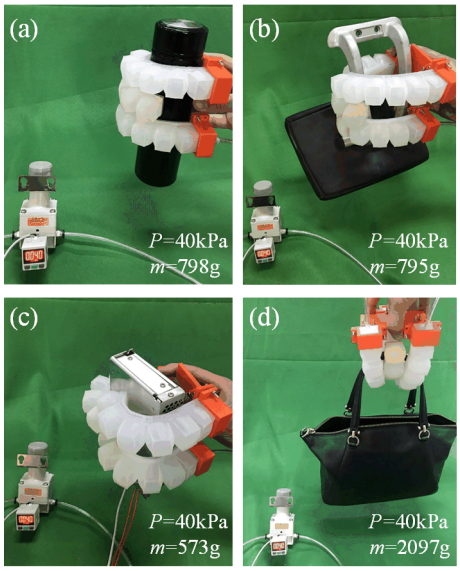

FIGURE 10. Grasping test of the capturing mechanism: (a) Longitudinal grasping of cylindrical object. (b) Longitudinal grasping of irregular object. (c) Lateral grasping of cubic object. (d) Surround holding of small section object.

the other actuators, but it also needs much higher pressure to generate large bending angle. This continuous structure makes the actuator has lower bending efficiency.

Through comparison, it is shown that the new actuator has a high bending angle and output force at low pressure, this demonstrates its excellent bending capacity.

E. GRASPING TEST

A three-jaw capturing mechanism was fabricated with three FBAs. According to the bearing capacity of the actuators, the grasping ability of the mechanism was tested in the range of 0kPa-40kPa. The actuators were distributed face to face for grasping objects with different shapes and contours.

1) LONGITUDINAL GRASPING

This grasping strategy targets objects with long longitudinal length and short lateral length. The objects will be enwound by the actuators and finally fixed to the installation base. The actuators and the base form a reliable shape and force closure, so the objects can achieve stable grasp. As shown in Fig.10 (a) and Fig.10 (b), the soft mechanism can realize the grasping of objects with cylindrical shape and irregular shape under the pressure of 40kPa. The grasping weight of this strategy could reach as much as 798g, its lateral grasping size ranged from 35mm to 100mm, and its longitudinal grasping size ranged from 0 to 65mm.

2) LATERAL GRASPING

This grasping strategy mainly handles at objects with big lateral dimension. Differring from the longitudinal grasping, the objects can only contact with the actuators, and the grasping force comes from the friction. Without the support of the installation base, load capacity of the mechanism greatly declines. As shown in Fig.10 (c), under the pressure of 40kPa, the largest grasping weight reaches 573g. With adaptability of the soft mechanism, it can realize the grasping of objects with different shapes. Its lateral grasping size ranges from 0mm to 50mm and its longitudinal grasping size ranges from 65mm to 120mm.

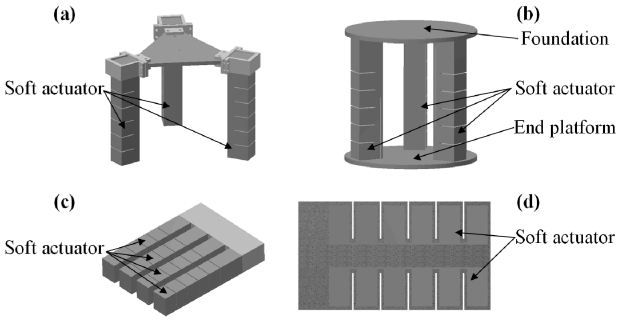

FIGURE 11. Application of the soft actuator: (a) Soft gripper. (b) Parallel end platform. (c) Rehabilitation glove (d) Actuator of bionic fish.

3) HANGING GRASPING

This grasping strategy mainly aimes at objects with small section dimension. Though the load capacity of the actuators is limited, the largest bending angle of the actuators can reach as much as 180 degree when the grasping space between actuators and the installation base are minimum. When the section dimension of the grasped objects is smaller than the minimum grasping dimension, motion of the objects is limited in the space; but there are no grasping forces applied to their surfaces. As shown in Fig.10 (d), under the pressure of 40kPa, the mechanism can hold an object as heavier as 2097g, its grasping section dimension ranges from 0mm to 30mm.

F. POTENTIAL APPLICATION

Because of the excellent bending capacity and softness, the actuator is promising in practical application with different configuration combinations as it is shown in Fig.11.

Fig.11 (a) shows a soft gripper composed of three actuators. The three actuators is drived at the same time to accomplish the grasping motion. Because of the softness of the actuators, the soft gripper has good adaptability. It can be used for grasping fragile objects or living objects. Fig.11 (b) shows a parallel end platform. Three soft actuators are installed parallel between the foundation and the end platform. By controlling the movement of each actuator, the end platform can achieve a given attitude. This platform can be used in environment detection. Fig.11 (c) shows a soft rehabilitation glove composed of four actuators. Once pressured, the actuators offer force to help rehabilitation of the patients. Fig.11 (d) presents a drive method of bionic fish. Two soft actuators are installed back to back. Through driving the two actuators, the bionic fish is propelled forward or turn.

V. CONCLUSION

This article proposes a novel segmented soft pneumatic actuator with large bending angle and large output force. Through finite-element analysis, it is shown that FBA has

significantly improved its bending angle and output force compared with CBA. Upon the completion of the design of the chamber structure, key parameters of the actuator have been further optimized by simulation. Several actuator samples were fabricated with multi-step molding methods, and all the molds were 3-D printed. A test platform was established, by which bending angles and output forces were tested. Besides, a novel curve fitting method has been proposed to obtain the bending angle of the actuator. A three-jaw soft mechanism was fabricated. According to different shapes and dimensions of the grasped objects, three kinds of grasping strategy have been proposed. The grasping ability of each strategy are analyzed, which demonstrates the excellent adaptability and grasping capacity of the mechanism.

The newly developed FBA greatly improves the bending angle and output force, however there are still some problems to be further studied. Stiffness of the actuator is insufficient, its output force is still limited, and particle strengthening or variable stiffness material may be a promising method to overcome these defects. For objects with different shapes and dimensions, how to plan the grasping strategy and path to realize the reliable grasp is a interesting problem to be further investigated.

REFERENCES

[1] M. Manti, T. Hassan, G. Passetti, N. D'Elia, C. Laschi, and M. Cianchetti, "A bioinspired soft robotic gripper for adaptable and effective grasping," *Soft Robot.*, vol. 2, no. 3, pp. 107–116, Sep. 2015.

[2] Z. Y. Zhang, X. Wang, S. Wang, D. Meng, and B. Liang, "Design and modeling of a parallel-pipe-crawling pneumatic soft robot," *IEEE Access*, vol. 7, pp. 134301–134317, 2019.

[3] R. F. Shepherd, F. Ilievski, W. Choi, S. A. Morin, A. A. Stokes, A. D. Mazzeo, X. Chen, M. Wang, and G. M. Whitesides, "Multigait soft robot," *Proc. Nat. Acad. Sci. USA*, vol. 108, no. 51, pp. 20400–20403, Dec. 2011.

[4] Y. Hao, Z. Gong, Z. Xie, S. Guan, X. Yang, T. Wang, and L. Wen, "A soft bionic gripper with variable effective length," *J. Bionic Eng.*, vol. 15, no. 2, pp. 220–235, Mar. 2018.

[5] J. Li, J. He, Y. Wang, K. Yu, M. Wozniak, and W. Wei, "A biomimetic flexible fishtail embedded with shape memory alloy wires," *IEEE Access*, vol. 7, pp. 166906–166916, 2019.

[6] H.-T. Lin, G. G. Leisk, and B. Trimmer, "GoQBot: A caterpillar-inspired soft-bodied rolling robot," *Bioinspiration Biomimetics*, vol. 6, no. 2, Jun. 2011, Art. no. 026007.

[7] M. Cianchetti, V. Mattoli, B. Mazzolai, C. Laschi, and P. Dario, "A new design methodology of electrostrictive actuators for bio-inspired robotics," *Sens. Actuators B, Chem.*, vol. 142, no. 1, pp. 288–297, 2009.

[8] L. Shi, S. Guo, M. Li, S. Mao, N. Xiao, B. Gao, Z. Song, and K. Asaka, "A novel soft biomimetic microrobot with two motion attitudes," *Sensors*, vol. 12, no. 12, pp. 16732–16758, Dec. 2012.

[9] N. W. Bartlett, M. T. Tolley, J. T. B. Overvelde, J. C. Weaver, B. Mosadegh, K. Bertoldi, G. M. Whitesides, and R. J. Wood, "A 3D-printed, functionally graded soft robot powered by combustion," *Science*, vol. 349, no. 6244, pp. 161–165, Jul. 2015.

[10] R. F. Shepherd, A. A. Stokes, J. Freake, J. Barber, P. W. Snyder, A. D. Mazzeo, L. Cademartiri, S. A. Morin, and G. M. Whitesides, "Using explosions to power a soft robot," *Angew. Chem. Int. Ed.*, vol. 52, no. 10, pp. 2892–2896, Mar. 2013.

[11] C. Laschi, B. Mazzolai, and M. Cianchetti, "Soft robotics: Technologies and systems pushing the boundaries of robot abilities," *Sci. Robot.*, vol. 1, no. 1, 2016, Art. no. eaah3690.

[12] A. D. Marchese, R. K. Katzschmann, and D. Rus, "A recipe for soft fluidic elastomer robots," *Soft Robot.*, vol. 2, no. 1, pp. 7–25, Mar. 2015.

[13] Y. Fei, J. Wang, and W. Pang, "A novel fabric-based versatile and stiffness-tunable soft gripper integrating soft pneumatic fingers and wrist," *Soft Robot.*, vol. 6, no. 1, pp. 1–20, Feb. 2019.

[14] Z. Wu, X. Li, and Z. Guo, "A novel pneumatic soft gripper with a jointed endoskeleton structure," *Chin. J. Mech. Eng.*, vol. 32, no. 1, p. 78, Dec. 2019.

[15] D. Rus and M. T. Tolley, "Design, fabrication and control of soft robots," *Nature*, vol. 521, no. 7553, pp. 467–475, May 2015.

[16] G. Krishnan, "Kinematics of a new class of smart actuators for soft robots based on generalized pneumatic artificial muscles," in *Proc. IEEE/RSJ Int. Conf. Intell. Robots Syst.*, Chicago, IL, USA, Sep. 2014, pp. 587–592.

[17] P. Polygerinos, Z. Wang, J. T. B. Overvelde, K. C. Galloway, R. J. Wood, K. Bertoldi, and C. J. Walsh, "Modeling of soft fiber-reinforced bending actuators," *IEEE Trans. Robot.*, vol. 31, no. 3, pp. 778–789, Jun. 2015.

[18] B. Mosadegh, P. Polygerinos, C. Keplinger, S. Wennstedt, R. F. Shepherd, U. Gupta, J. Shim, K. Bertoldi, C. J. Walsh, and G. M. Whitesides, "Pneumatic networks for soft robotics that actuate rapidly," *Adv. Funct. Mater.*, vol. 24, no. 15, pp. 2163–2170, Apr. 2014.

[19] F. Ilievski, A. D. Mazzeo, R. F. Shepherd, X. Chen, and G. M. Whitesides, "Soft robotics for chemists," *Angew. Chem. Int. Ed.*, vol. 50, no. 8, pp. 1890–1895, 2011.

[20] P. Polygerinos, S. Lyne, Z. Wang, L. F. Nicolini, B. Mosadegh, G. M. Whitesides, and C. J. Walsh, "Towards a soft pneumatic glove for hand rehabilitation," in *Proc. IEEE/RSJ Int. Conf. Intell. Robots Syst.*, Tokyo, Japan, Nov. 2013, pp. 1512–1517.

[21] K. C. Galloway, K. P. Becker, B. Phillips, J. Kirby, S. Licht, D. Tchernov, R. J. Wood, and D. F. Gruber, "Soft robotic grippers for biological sampling on deep reefs," *Soft Robot.*, vol. 3, no. 1, pp. 23–33, Mar. 2016.

[22] G. Zhong, Y. Hou, and W. Dou, "A soft pneumatic dexterous gripper with convertible grasping modes," *Int. J. Mech. Sci.*, vols. 153–154, pp. 445–456, Apr. 2019.

[23] Y. Chen, S. Guo, C. Li, H. Yang, and L. Hao, "Size recognition and adaptive grasping using an integration of actuating and sensing soft pneumatic gripper," *Robot. Auto. Syst.*, vol. 104, pp. 14–24, Jun. 2018.

[24] J. Shintake, V. Cacucciolo, D. Floreano, and H. Shea, "Soft robotic grippers," *Adv. Mater.*, vol. 30, no. 29, Jul. 2018, Art. no. 1707035.

[25] H. K. Yap, P. M. Khin, T. H. Koh, Y. Sun, X. Liang, J. H. Lim, and C.-H. Yeow, "A fully fabric-based bidirectional soft robotic glove for assistance and rehabilitation of hand impaired patients," *IEEE Robot. Autom. Lett.*, vol. 2, no. 3, pp. 1383–1390, Jul. 2017.

[26] Y. Sun, Y. Seong Song, and J. Paik, "Characterization of silicone rubber based soft pneumatic actuators," in *Proc. IEEE/RSJ Int. Conf. Intell. Robots Syst.*, Nov. 2013, pp. 4446–4453.

[27] Y. F. Hao, T. Wang, Z. Ren, Z. Gong, H. Wang, X. Yang, S. Guan, and L. Wen, "Modeling and experiments of a soft robotic gripper in amphibious environments," *Int. J. Adv. Robot. Syst.*, vol. 14, no. 3, 2017, Art. no. 1729881417707148.

[28] L. Rosalia, B. W.-K. Ang, and R. C.-H. Yeow, "Geometry-based customization of bending modalities for 3D-printed soft pneumatic actuators," *IEEE Robot. Autom. Lett.*, vol. 3, no. 4, pp. 3489–3496, Oct. 2018.

[29] W. Park, S. Seo, and J. Bae, "A hybrid gripper with soft material and rigid structures," *IEEE Robot. Autom. Lett.*, vol. 4, no. 1, pp. 65–72, Jan. 2019.

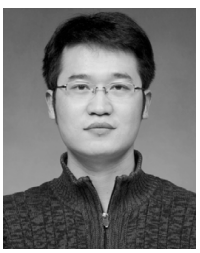

FEI YANG was born in Yuncheng, Shanxi, in 1985. He received the B.S. degree in mechanical design and theory from Guizhou University, Guiyang, in 2007, and the M.S. and Ph.D. degrees in mechanical design and theory from the Harbin Institute of Technology, Harbin, China, in 2014. From 2014 to 2017, he was a Research Assistant with the Harbin Institute of Technology. He was an Associate Professor, in 2017. His main research interests include wheeled planetary vehicle mobility and space capture.

QI RUAN received the B.S. and M.S. degrees in mechanical design and theory from the Harbin Institute of Technology, Harbin, China, in 2011 and 2013, respectively, where he is currently pursuing the Ph.D. degree in aerospace science and technology. He was with the Beijing Institute of Satellite Environment Engineering, Beijing, China, from 2013 to 2017. His main research interests include soft robot and adaptive space capturing mechanism.

YIMING MAN was born in Hubei, in 1982. He received the B.S. degree in thermal energy and power engineering from Jiangsu University, Zhenjiang, Jiangsu, and the M.S. and Ph.D. degrees in vehicle engineering from the Beijing Institute of Technology, Beijing. He was a Senior Engineer, in 2014. His main research interest includes aircraft design.

ZHIJIE XIE received the Ph.D. degree from the Harbin Institute of Technology, in 2014. He is currently a Lecturer of aerospace science and technology. His research interests include development of mechanical basic components and the research of space capture mechanism on orbit.

HONGHAO YUE was born in 1978. He is currently a Professor and a Ph.D. Supervisor with the Research Center of Aerospace Mechanism Control, Harbin Institute of Technology, China. More than 40 academic articles have been published in international famous periodicals and important international academic conferences. He has also published one English Publication. He holds four national invention patents. His main research interests include mechatronics engineering and active vibration control of smart structures. He received one award, two national technological inventions, and two first prize of Heilongjiang's Technological Invention, and one Science and Technology Progress of the Whole Army (two awards).

BING LI (Senior Member, IEEE) received the Ph.D. degree in mechanical design and theory from the Harbin Institute of Technology, Harbin, China, in 1999. He is currently a Professor and a Ph.D. Supervisor with the Harbin Institute of Technology (Shenzhen), Shenzhen, China. More than 70 academic articles have been published in international famous periodicals and important international academic conferences. His main research interests include parallel robot, space folding mechanism, and mechanical vibration and control. He is a member of ASME. He serves as an Associate Editor for *Intelligent Service Robotics*.

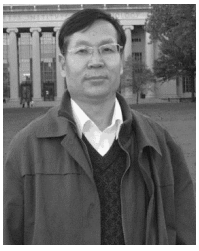

RONGQIANG LIU (Member, IEEE) received the Ph.D. degree in mechanical design and theory from the Harbin Institute of Technology, Harbin, China, in 1995. He is currently a Professor and a Ph.D. Supervisor with the Research Center of Aerospace Mechanism Control, Harbin Institute of Technology. His main research interests include wearable robot, space folding mechanism, and lunar rover. He is an Executive Member of the Space Mechanics Committee of Chinese Space Association.